ARTICLE IN PRESS

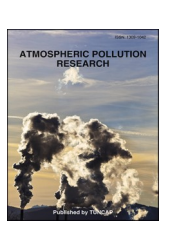
Atmospheric Pollution Research xxx (xxxx) xxx

ELSEVIER

Contents lists available at ScienceDirect

Atmospheric Pollution Research

journal homepage: www.elsevier.com/locate/apr



Air quality affected by biomass burning at the Paraná River Delta on rural and industrial coastal areas of greater Rosario, Argentina

M.V. Binet ^{a,b,*}, G.A. Piñol ^{a,b}, M.F. Valle Seijo ^{a,b}, M.I. Micheletti ^{a,c}, R.D. Piacentini ^{a,d}

- ^a Instituto de Física Rosario (CONICET Universidad Nacional de Rosario), Rosario, Argentina
- b Facultad de Química e Ingeniería del Rosario, Pontificia Universidad Católica Argentina (UCA), Av. Pellegrini 3314, (S2002QEO), Rosario, Argentina
- Facultad de Ciencias Bioquímicas y Farmacéuticas, Universidad Nacional de Rosario, UNR, Suipacha 531, (2000), Rosario, Argentina
- d Facultad de Ciencias Exactas, Ingeniería y Agrimensura, Universidad Nacional de Rosario, Rosario, Argentina

ARTICLE INFO

Keywords: Air quality Fires Greater Rosario NO₂ CO AOD

ABSTRACT

Biomass combustion releases various gaseous pollutants and aerosol particles, impacting human health and climate. This study evaluates the effects of biomass burning in the Paraná River Delta on air quality in coastal areas of Greater Rosario, Argentina, focusing on the industrial site of San Lorenzo (SL) and the rural site of Fighiera (FI), from September 6 to 17, 2022. The research examines the transport of pollutants, specifically NO_2 , CO, and (total and Black Carbon) aerosols, and their correlations. During this period, the Tropospheric Vertical Column Density (VCDtrop) for NO_2 peaked at over 1.40×10^{16} molecules/cm² in Fighiera on September 16, 2022, while CO reached 3.29×10^{18} molecules/cm² in San Lorenzo on September 13, 2022. Aerosol optical depth (AOD) exceeded 0.5 at both sites on September 13, 2022, linked to air masses from the fire-affected region. Additionally, the Fire Radiative Power (FRP) of the fires reached approximately 10 GW on September 13, 2022. A comparison with non-fire periods revealed that Fighiera, typically showing good air quality with lower pollutant levels than San Lorenzo, experienced a rise in pollutant concentrations during the biomass burning events, highlighting the significant impact of fire on local air quality.

1. Introduction

South America contains the largest area of wetlands globally, with the most extensive regions comprised of fluvial wetlands associated with the Amazon, Orinoco, and Paraguay-Paraná river systems (Junk et al., 2013).

In the central region of the Paraná River Delta, in front of the coastal zone of Greater Rosario in Santa Fe Province, Argentina, fires are a recurring phenomenon, of particularly high intensity and frequency from July to September during drought years. These fires are driven by a combination of anthropogenic activities and natural processes, including the La Niña phenomenon, which induces drought conditions (Binet et al., 2024; National Meteorological Service, 2022; Valle Seijo et al., 2024). The resulting reduction in the Paraná River's water levels, coupled with the formation of low-humidity vegetated areas, significantly enhances the risk of fire spread across vast regions, threatening the local flora and fauna and becoming a major health problem for the exposed populations.

Biomass combustion results in the emission of gaseous pollutants, including Carbon Dioxide (CO₂), Carbon Monoxide (CO), Nitrogen Oxides (primarily NO, which oxidizes to NO2 in the atmosphere, and their sum, NO_X), and Methane (CH4), as well as particulate matter (Urbanski, 2014). During fire events, Black Carbon (BC), a component of fine particulate matter especially risky for health, is highly enhanced (Guerrero et al., 2024). This fraction has a diameter up to 2.5 µm; when inhaled by humans, it is retained in the pulmonary alveoli, potentially triggering health issues, primarily related to the respiratory and cardiovascular systems. Global studies have identified strong links between both acute and chronic exposure to ambient PM2.5 and a range of negative health effects, including respiratory and cardiovascular diseases, neurological disorders, and increased risk of premature mortality (Brook et al., 2010; Casanova et al., 2016). For instance, Brook et al. (2010) provide an update on the scientific statement from the American Heart Association, emphasizing the cardiovascular risks associated with particulate matter. Meanwhile, Casanova et al. (2016) reveal local brain structural alterations linked to ambient fine particles in older women,

https://doi.org/10.1016/j.apr.2025.102712

Received 6 February 2025; Received in revised form 1 August 2025; Accepted 20 August 2025 Available online 21 August 2025

1309-1042/© 2025 Turkish National Committee for Air Pollution Research and Control. Published by Elsevier B.V. All rights are reserved, including those for text and data mining, AI training, and similar technologies.

Please cite this article as: M.V. Binet et al., Atmospheric Pollution Research, https://doi.org/10.1016/j.apr.2025.102712

^{*} Corresponding author. Instituto de Física Rosario (CONICET – Universidad Nacional de Rosario), Rosario, Argentina. E-mail address: binet@ifir-conicet.gov.ar (M.V. Binet).

M.V. Binet et al.

highlighting neurological impacts (see Fig. 1).

This study analyzes the levels of Atmospheric Vertical Column Densities (VCDs) for CO and Tropospheric Vertical Column Densities (VCDs_{trop}) for NO₂, along with burning aerosols, transported by air masses originating from fires in the Paraná Delta. These pollutants reached the city of San Lorenzo (SL) and the town of Fighiera (FI), located in the Northwest and Southeast coastal regions of Greater Rosario, respectively (as shown in Fig. 2). San Lorenzo is characterized by significant industrial activity, particularly the cereal industry, while Fighiera is a rural site with minimal industrial presence and low vehicular traffic. The primary aim of this study is to identify and characterize the impact on air quality, focusing on NO2, CO, and aerosols, in the coastal areas of Greater Rosario, specifically in San Lorenzo (North zone) and Fighiera (South zone), resulting from biomass burning in the islands of the Paraná Delta during the critical period from September 6 to 17, 2022. The study aims to address several key aspects to comprehensively understand the impact of fires on air quality. The analysis includes daily $NO_2\ VCD_{trop}$ and $CO\ VCD$, both of them detected by the TROPOspheric Monitoring Instrument (TROPOMI) on board the European Space Agency (ESA) Sentinel-5 Precursor satellite. These values are compared with those recorded during the same period in 2019, when no fires occurred in the Paraná Delta. Additionally, the behavior of these gases is analyzed for both sites during the period from 2019 to 2023 showing that San Lorenzo consistently exhibits higher levels of NO2 VCD_{trop} and CO VCD compared to Fighiera over time, except during special occasions.

Furthermore, the study examines the aerosol optical depth (AOD) provided by the Moderate Resolution Imaging Spectroradiometer (MODIS) instruments aboard the Terra and Aqua satellites, using the Multi-angle Implementation of Atmospheric Correction (MAIAC), and also assess the AOD for the black carbon fraction as detected by the Copernicus Atmosphere Monitoring Service (CAMS) model. The analysis of aerosol types and the Ångström Exponent is conducted using data from the Visible Infrared Imaging Radiometer Suite (VIIRS) aboard the Suomi National Polar-orbiting Partnership (S-NPP) satellite (https://www.nasa.gov/mission_pages/NPP/main/index.html). Increases in the values of the analyzed pollutant gases and aerosols during the study period from September 6 to 17, 2022, compared to the same period in 2019, are identified and quantified.

In order to evaluate the intensity of the fires at the Paraná River Delta in front of Greater Rosario, that potentially generated the analyzed pollutants, the Fire Radiative Power (FRP) is assessed.

2. Methodology

2.1. Study area

Greater Rosario also known as Rosario Metropolitan Region (RMR) is an area encompassing 27,559 $\,\mathrm{km}^2$ that includes Rosario City, of 1.029.619 inhabitants (INDEC, 2022), and smaller towns, as well as agricultural areas among them. It is located in the Southeastern part of Santa Fe Province on the right bank of the Paraná River, as shown in Fig. 2 Left.

The city of San Lorenzo, located in Greater Rosario, 24 km north of Rosario City, and designated as SL in Fig. 2 Middle and Right, spans over an area of $32~\rm km^2$ and has an estimated population of 50,954 inhabitants (INDEC, 2022). It has an average elevation of approximately $23–25~\rm m$ above sea level, with minimum values near $-2~\rm m$ and maximum elevations reaching around $37~\rm m$. The topography is predominantly flat to gently undulating, exhibiting minimal altitudinal variation across the urban and peri-urban areas. This city is a major global agro-export hub and belongs to one of the most important industrial areas in Santa Fe Province, with an extensive network of modern private docks and shipping terminals that facilitate the export of much of the country's grain, oilseeds, oils, fuels, hydrocarbons, minerals, chemicals, and petrochemicals.

On the other hand, the town of Fighiera covers a territorial extension of 137.9 km², mostly rural and with a small residential area of approximately 3.3 km². It is located 37 km south of Rosario and is designated as FI in Fig. 2 Middle and Right. It has a population of 5962 inhabitants (INDEC, 2022). Prominent institutions in the municipality include the Senior Citizens' Center, the Primary School, the Secondary School, the Church of Nuestra Señora del Luján, two sports clubs, and the Potable Water Cooperative. The town lies within the vast Pampas plain and exhibits a nearly flat topography, with altitudes generally below 30 m above sea level and in close proximity to the Paraná River. Fighiera and San Lorenzo form part of the so-called Pampa Ondulada (Undulating Pampas) or Fluvial Diagonal, a geomorphological subregion characterized by gentle slopes (altitudinal differences typically less than 5 m), shallow valleys and depressions, and areas prone to water accumulation during flood events, particularly those associated with the Pavón River.



Fig. 1. Aerial view of Rosario City center showing the smoke on September 14, 2022, at 09:30 local hours (UT-3 h). Photo captured by Nahuel Rullo

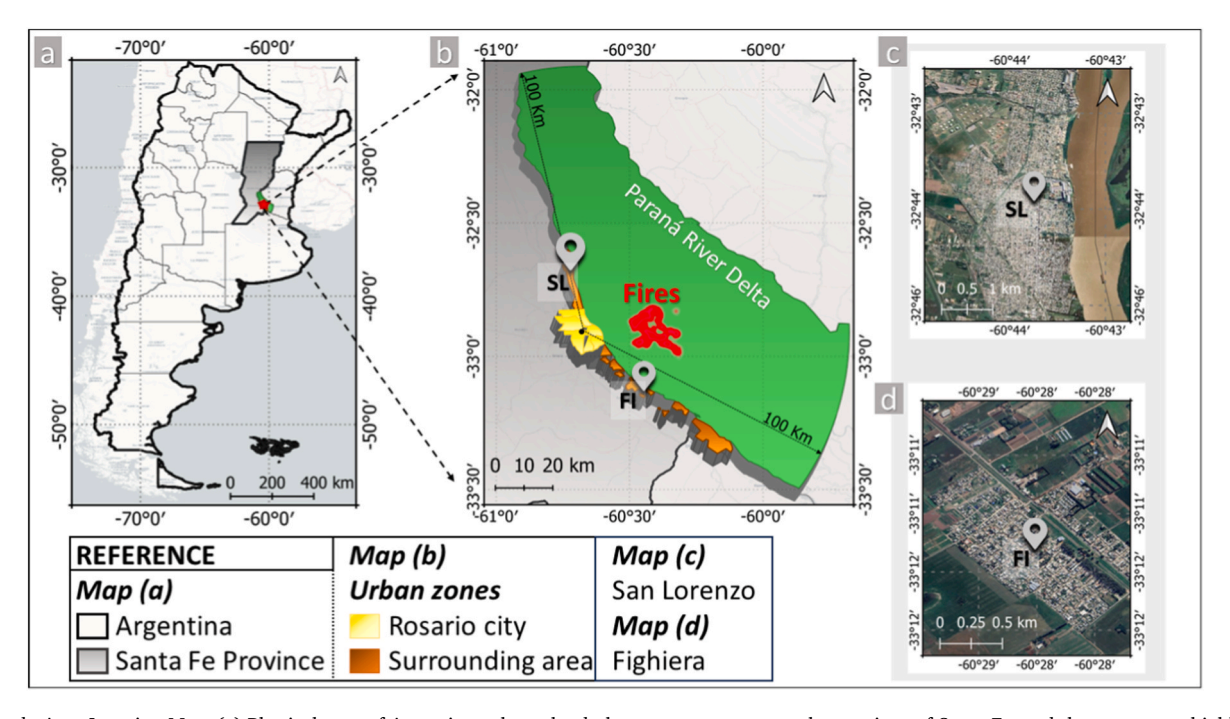


Fig. 2. Study Area Location Map. (a) Physical map of Argentina, where the dark gray area represents the province of Santa Fe, and the green area highlights the portion of the Paraná Delta considered in this study. (b) Enlargement of the Paraná Delta region, showing the city of Rosario (yellow area) and nearby populated areas (brown area). The locations of San Lorenzo (SL) and Fighiera (FI) are marked with gray symbols. (c) Aerial view of San Lorenzo city. (d) Aerial view of Fighiera town. Source for Figures c and d: Google Earth Pro.

The Paraná River Delta, situated at the terminus of the La Plata Basin, is recognized as a macrosystem of wetlands, spanning approximately $17,000~\mathrm{km}^2$ across the provinces of Entre Ríos (comprising 80~% of the area), Buenos Aires (15~%), and Santa Fe (5~%) (Astrada et al., 2010), being the relative location between these provinces depicted in Fig. 2. Greater Rosario, located in the Southeastern part of this basin, encompasses a coastal area in front of a portion of the Paraná River Delta.

In this study, we focus on a specific region within the Paraná Delta, defined by a 100 km radius around the city of Rosario (-32.95, -60.69, 25 m a.s.l.). The area selected for this study covers 8677.35 km^2 , representing 61.98% of the entire Paraná Delta, predominantly covering the Middle Delta region. This area is particularly relevant due to the significant impact of fire events on the air quality of Rosario and its neighboring regions, owing to their geographic proximity. The boundary polygon of the Paraná Delta was obtained from the Spatial Data Infrastructure of the Argentine Republic (IDERA) and subsequently refined to reflect the intersection of the Paraná Delta with the 100 km radius around Rosario. Additional characteristics of this study area are detailed in Binet et al. (2024).

2.2. NO2 VCDtrop and CO VCD data

The Sentinel-5 Precursor operates in a Sun-synchronous orbit, providing near-complete daily coverage of the Earth's surface with a local equatorial overpass time of approximately 13:30. The instrument's four spectrometers cover the solar spectrum in the ultraviolet–visible (UV–vis, 270–500 nm), near-infrared (NIR, 675–775 nm), and shortwave infrared (SWIR, 2305–2385 nm) (Veefkind et al., 2012). TRO-POMI NO2 columns are derived from the UV–vis spectrometer in the wavelength range of 405–465 nm, with an initial spatial resolution of 3.5 km \times 7 km, improved to 3.5 km \times 5.5 km as of August 2019 (Oelker et al., 2022). The CO VCD from TROPOMI is estimated using spectral radiance measurements in the shortwave to infrared spectral ranges around 2.3 μ m, which are sensitive to CO absorption. This data is provided with a daily resolution of 5.5 km \times 7 km (Landgraf et al., 2016a,b; Borsdorff et al., 2018). This enhancement allows for better detection of

air pollution over cities. For this study, the TROPOMI Sentinel-5 Precursor Level 2 offline products, (S5P_OFFL_L2_NO2_) and (S5P_OFFL_L2_CO_), were used. Data from September 2019 (without fires) and September 2022 (with fires) were analyzed. Data with quality assurance (QA) values above 0.75 were selected for NO $_2$ VCDtrop, and QA values above 0.5 were used for CO VCD. The NO $_2$ VCD $_{trop}$ and CO VCD values were then averaged from a 3x3 pixel grid. In the NO $_2$ maps, a filter with a QA value greater than 0.5 was used to obtain a clearer depiction of the NO $_2$ plume. This decision was made because a QA value above 0.75 corresponds to a filter with a cloud radiance fraction exceeding 0.5, which complicates the differentiation between smoke and clouds in areas affected by fire.

2.3. Aerosol optical depth (AOD) and black carbon (BC) AOD

AOD values at 470 nm, were derived from the MODIS Blue band B3 (0.47 $\mu m)$ provided by the MCD19A2 Version 6.1 product. This dataset is accessible through NASA's data distribution platforms. Comprehensive details regarding the product's capabilities, limitations, and recent advancements are outlined by Lyapustin et al. (2011, 2012, 2018). The MCD19A2 product delivers a daily temporal resolution, with a fine spatial resolution of 1 km \times 1 km. Its temporal coverage extends from February 24, 2000, to the present, and it encompasses a global spatial extent.

To ensure data quality, AOD values were filtered using the Quality Assurance (QA) dataset, focusing on Bits 0–2 of the Cloud Mask. For this study, only AOD values corresponding to Cloud Mask categories "Clear" or "Possibly Cloudy" were included.

AOD at 550 nm within the visible spectrum serves as an indicator of the total aerosol content in the atmospheric column, which includes components such as desert dust, sea salt, sulfate, organic matter, and black carbon. To represent wildfire aerosols, we utilize Black Carbon (BC) AOD as estimated by the Copernicus Atmosphere Monitoring Service (CAMS) reanalysis (Inness et al., 2019), of the European Union, a component of the Copernicus Earth observation program (https://www.copernicus.eu/en), produced by the European Centre for Medium-Range

M.V. Binet et al.

Weather Forecasts (ECMWF). Previous studies used this product to estimate wildfire aerosols, as in Tang et al. (2021). Black Carbon values were calculated for 12 UTC (local time: 09:00) with a resolution of 40 km. The reanalysis model was used as a proxy for wildfire aerosols. CAMS combines satellite observations of atmospheric composition with detailed computer simulations of the atmosphere using a method called data assimilation.

The selection of the CAMS reanalysis to estimate BC AOD was based on its global availability, temporal continuity, and proven applicability for evaluating wildfire-related aerosols in regional-scale studies. Compared to other atmospheric composition models such as GEOS-Chem, or WRF-Chem, CAMS offers several advantages, including direct access to ready-to-use BC AOD products derived from the assimilation of multiple satellite datasets without the need for high computational resources or complex model configurations. Although CAMS is typically used to study large-scale aerosol transport, in this work it was employed as a complementary estimate to provide a general characterization of atmospheric black carbon behavior during wildfire events. While its spatial resolution (~40 km) does not allow for detailed analysis of local variations, the data are useful for identifying trends and supporting joint interpretation with other satellite products.

2.4. Fire Radiative Power (FRP)

A key variable that characterizes the energy radiated by a fire is the Fire Radiative Power (FRP). This metric reflects the immediate radiative energy released over a specific area by actively burning fires and is associated with the rate of biomass combustion (Wooster et al., 2003), as well as the emission rates of trace gases and aerosols (Kaiser et al., 2012; Wan et al., 2023). The FRP data are provided by the VIIRS thermal anomalies/active fire product, which has a spatial resolution of 375 m. Due to the unique spatial and spectral resolution of the data, the VIIRS 375 m fire detection algorithm has been specifically tailored and fine-tuned to improve its accuracy for detecting small fires while minimizing false alarms, as detailed on the Earth Data-NASA website (http://www.earthdata.nasa.gov/learn/find-data/near-real-time/firms/viirs-i-band-375-m-active-fire-data/).

These data are collected by sensors aboard both the joint NASA/NOAA S-NPP satellite and the NOAA-20 satellite. The FRP represents the pixel-integrated power radiated by fires in units of Megawatts (MW). A Fire Mask was applied by selecting only those pixels with nominal (8) and high (9) confidence levels. Pixels with low confidence (7) were excluded, as these thermal anomalies lack sufficient quality to be reliably identified as active fires. The discarded pixels include: those not processed due to data acquisition loss; bowtie or edge pixels (pixels located in the marginal areas of the image, where the satellite sensor's accuracy is typically lower); water-covered areas; cloud-covered pixels; land pixels with no fire detection; and pixels with insufficient background information to allow for accurate classification.

2.5. Meteorological data

The data were derived from the "ERA5-Land hourly data from 1950 to present" from: 2m temperature, 10m u and v components of wind (the eastward and northward horizontal wind speed components, respectively, at a height of 10 m above ground level), surface pressure with a spatial resolution of $0.1^{\circ} \times 0.1^{\circ}$ (Muñoz Sabater, J 2019) and "ERA5 hourly data on pressure levels from 1940 to present" (Hersbach et al., 2023) from relative humidity with a spatial resolution of $0.25^{\circ} \times 0.25^{\circ}$. As no weather stations data are available in Fighiera and San Lorenzo, the meteorological characterization of the sites was carried out using ERA5 data (Ghasempour et al., 2021).

3. Results

3.1. Wildfires

Table 1 presents the data for the hole period studied, where can be seen the evolution of the fires in Paraná River Delta, reaching the peaks of Hotspots, Burned Area and FRP on September 12, 13 and 16, 2022. The information was obtained from the Fire Information for Resource Management System (FIRMS) website of NASA (https://firms.modaps.eosdis.nasa.gov/), with data provided by the VIIRS instrument aboard the SUOMI/NOAA satellites.

The burned area (BA) is obtained by multiplying the number of daily fire hotspots by the size of a pixel, which is equivalent to $0.141~\rm km^2$. This value is calculated based on the side length of the pixel provided by VIIRS: $0.375~\rm km$ * $0.375~\rm km$ (Museo Scasso, 2021).

From this information, it can be observed that September 13 was the most critical in terms of the number of detected heat spots, burned area and FRP. On the same day, high values of NO_2 , CO, AOD and Black Carbon were observed in San Lorenzo.

The significant impact of the fires on the wetland soil can be observed in Fig. 3 for September 13, 2022, a critical day marked by the highest number of detected heat spots and maximum FRP values approaching 10 GW.

3.2. Meteorology of the analyzed period

Table 2 provides a summary of the statistics derived from meteorological data for the study period. Given that Fighiera and San Lorenzo are approximately 55 km apart, no significant differences are observed in the values presented by ERA5 for the analyzed variables.

Throughout the analyzed period, the environment exhibited a notably dry condition, with the average relative humidity not exceeding 50 % in either of the two sites. Furthermore, there were no recorded precipitation events during this timeframe, creating an ideal scenario for the potential development of wildfires in the region. The selected dates belong to a period of three (3) consecutive years of drought caused by the La Niña event that started in 2020 (National Meteorological Service,

Table 1Days with the daily evolution of heat spots detected by the SUOMI NPP and NOAA-20 satellites in the Paraná Delta Islands, estimation of the burned area, and FRP.

Date	HP (1)	HP (2)	BA (1)	BA (2)	FRP (1)	FRP (2)
			[Km ²]	[Km ²]	[MW]	[MW]
September	1.00	1.00	0.14	0.14	13.47	4.84
6, 2022						
September	3.00	13.00	0.42	1.83	501.48	544.94
7, 2022						
September	15.00	17.00	2.12	2.40	214.49	235.22
8, 2022						
September	31.00	39.00	4.37	5.50	893.77	793.16
9, 2022						0=4.40
September	41.00	24.00	5.78	3.38	613.28	276.63
10, 2022 September	27.00	38.00	3.81	5.36	101.92	92.47
11, 2022	27.00	36.00	3.01	3.30	101.92	92.47
September	122.00	136.00	17.20	19.18	3386.22	2295.57
12, 2022						
September	220.00	428.00	31.02	60.35	3319.17	9002.61
13, 2022						
September	42.00	42.00	5.92	5.92	186.92	402.36
14, 2022						
September	27.00	15.00	3.81	2.12	489.06	359.89
15, 2022						
September	142.00	121.00	20.02	17.06	3001.21	3061.96
16, 2022						
September	3.00	39.00	0.42	5.50	23.22	335.37
17, 2022						

HP = hotspot; BA = burned area; (1) NOAA-20; (2) SUOMI NPP.

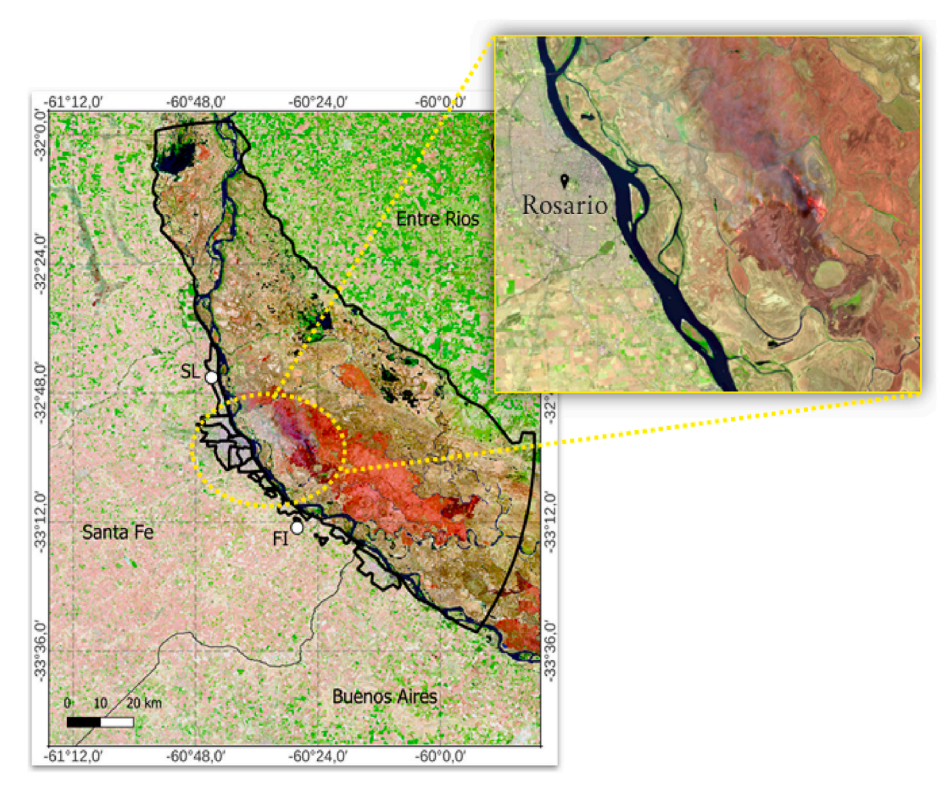


Fig. 3. Burned area identified using the SWIR spectral band combination (12, 8A, 4) on September 13, 2022. Source: Sentinel-2 L2A. The burned area on September 13, 2022, is equivalent to 3485 football fields.

Table 2General Statistics of Meteorological Data for the Analyzed Period: September 6–17, 2022. Data source: ERA5.

		San Lorenzo			Fighiera			
	T (°C)	RH(%)	P (hPa)	W _s (m/s)	T (°C)	RH(%)	P (hPa)	W _s (m/s)
Mean	15.86	45.83	1016.35	3.15	15.38	47.46	1017.59	2.81
St. Dev.	5.34	14.45	6.16	1.58	5.05	15.46	6.09	1.44
Max	27.36	77.02	1024.82	7.60	26.53	80.96	1025.66	7.18
Min	5.91	22.51	1000.77	0.20	5.58	22.31	1002.33	0.45

T = Temperature (°C); RH = Relative Humidity (%); P = Atmospheric Pressure (hPa); Ws = Wind Speed (m/s).

2020)

The mean temperature remained within the range of 15–16 $^{\circ}$ C, considered typical values for September in the area under study. The average wind speed was low, although peak values at both sites indicated moderate gusts.

3.3. Analysis of NO_2 VCD_{trop} and CO VCD detected in rural and industrial areas

 $NO_2 \ VCD_{trop}$ were obtained for the sites of Fighiera and San Lorenzo using TROPOMI. In Binet et al. (2024), the analysis revealed that $NO_2 \ VCD_{trop}$ levels in Fighiera reached the highest average concentration during the study period (3.42 \times 10^{15} molecules/cm²), surpassing those in the industrial area of San Lorenzo (2 \times 10^{15} molecules/cm²). A closer examination of daily $NO_2 \ VCD_{trop}$ data highlights September 16, 2022, as a key date influencing the mean values in Fighiera. On this day, $NO_2 \ VCD_{trop}$ in Fighiera was 15.42 times higher than in San Lorenzo (Fig. 4a).

During the fire period analyzed (September 6–17, 2022), CO VCD data revealed that on September 11 (+10 %), September 12 (+13 %), September 14 (+34 %), September 15 (+4 %), and September 16 (+102 %), CO VCD in Fighiera, as detected by TROPOMI, exceeded those observed in San Lorenzo (Fig. 4b). On September 13, though, San Lorenzo exhibited a CO VCD that was 94 % higher compared to Fighiera. An

increase in CO VCD was observed in San Lorenzo on September 8, but this rise is not related to the Paraná Delta fires. Instead, it is potentially linked to air currents that transported gases and particulate matter from fires located in the Northwest of Argentina, approximately 800 km away from the study area addressed in this work. Additionally, this increase may have been influenced by a low-level jet stream (SALLJ - Chaco Jet), which carries gaseous emissions from fires in Peru, Bolivia, Paraguay, and northeastern Argentina, particularly from Formosa and Chaco Provinces.

The missing data points in Fig. 4a–b correspond to specific dates where TROPOMI did not detect values. For FI, CO VCD data are missing on September 6, 8, and 10, 2022. For SL, CO VCD data are unavailable on September 10, 11, and 17, 2022. Regarding FI NO_2 VCD_{trop} data, the missing values occur on September 11 and 17, 2022. Similarly, for SL no NO_2 VCD_{trop} data are available on September 11 and 17, 2022.

3.4. Analysis of gas level peaks on September 13 and 16: evaluating satellite tools and models for understanding gas and aerosol plumes

Based on the gas data detected by TROPOMI, it is interesting to analyze what happened on September 13 and 16, when significant increases in CO and NO_2 levels were achieved in San Lorenzo and Fighiera, respectively, as shown in Fig. 4. To analyze these events, it is crucial to

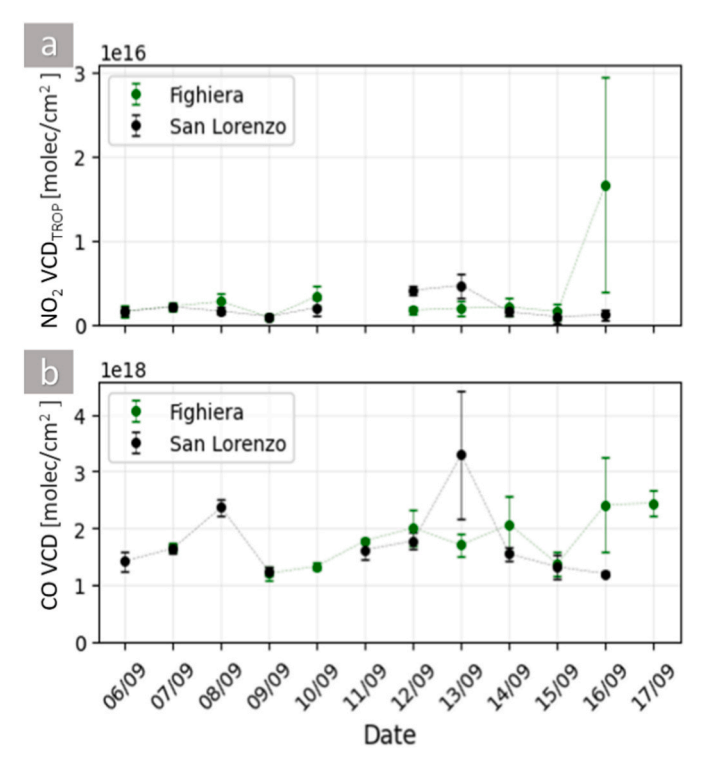


Fig. 4. Time series of gas levels, detected by TROPOMI, over Fighiera and San Lorenzo from September 6 to 17, 2022: (a) NO_2 VCD $_{trop}$ and (b) CO VCD.

evaluate different satellite tools and models to gain a detailed view of the situation, allowing for the correlation of various tools and the identification of potential sources of the gas and aerosol plumes that reached these locations. Among these tools, the analysis included the true-color imagery and heat point locations detected by the VIIRS instruments aboard the SUOMI NPP and NOAA-20 satellites, as well as the NO $_2$ VCDtrop and CO VCD data provided by TROPOMI.

Fig. 5a (top panel) shows that the emission plume travels towards the Northwest direction on September 13, 2022, reaching San Lorenzo, while the situation depicted in the bottom panel confirms the release of gas emissions from the fires towards the Southwest direction on September 16, 2022, impacting the town of Fighiera.

Data from TROPOMI highlights the NO_2 plume in red, passing through Fighiera on September 16, 2022, indicating the presence and transport of elevated NO_2 VCDtrop levels exceeding 1.60×10^{16} molecules/cm² (Fig. 5b, bottom panel). Additionally, Fig. 5c (bottom panel) shows the CO plume moving southwest, crossing over Fighiera.

The highest CO VCD, recorded at 3.29×10^{18} molecules/cm², was observed in San Lorenzo on September 13, 2022. During the analyzed fire period, Fighiera showed slightly higher average CO VCD values, reaching 1.79×10^{18} molecules/cm², surpassing San Lorenzo's value of 1.74×10^{18} molecules/cm² (Table 3). A higher standard deviation was noted in San Lorenzo, primarily driven by the elevated CO VCD detected on September 13, 2022.

The maximum NO $_2$ VCD $_{trop}$, recorded at 1.66×10^{16} molecules/cm 2 , was observed in Fighiera on September 16, 2022. In comparison to San Lorenzo, Fighiera displayed higher average NO $_2$ VCD $_{trop}$ values during the analyzed fire period, with a value of 3.42×10^{15} molecules/cm 2 , exceeding San Lorenzo's value of 2.00×10^{15} molecules/cm 2 (Table 3). Fighiera also had a higher standard deviation, primarily influenced by the elevated NO $_2$ VCD $_{trop}$ detected on September 16, 2022.

In Fighiera, at least 75 % of the CO VCD values (Q3) detected during the analyzed fire period (September 6–17, 2022) were equal to or less than 2.15 \times 10^{18} molecules/cm². In comparison, the corresponding value in San Lorenzo was 1.92×10^{18} molecules/cm². Regarding NO $_2$ VCD $_{trop}$ values, at least 75 % of them (Q3) detected in Fighiera during

the same period were equal to or less than 2.86×10^{15} molecules/cm², which was higher than the Q3 value for San Lorenzo (2.54×10^{15}).

The high CO VCD value attained in San Lorenzo on September 13, 2022, representing a 94 % increase compared to Fighiera on the same date, correlates with the plume of pollutant emissions moving from the fire sources towards San Lorenzo (Figs. 4b and 5c).

It can be observed from Fig. 5a that, while only the border of the emissions plume makes contact with San Lorenzo on September 13, the bulk of the plume traverses Fighiera on September 16. Consistent with this, Fighiera experienced significant increases in both NO₂ and CO on this date, as shown in Fig. 4. In contrast, San Lorenzo saw a noticeable increase only in CO when the contaminant plume bordered the city, with only a slight increase in NO₂. These results, as shown in Fig. 4, are consistent with the observations in Fig. 5b and c. While both NO₂ and CO exhibit elevated values across Fighiera on September 16, as depicted in the corresponding maps, only CO shows a significant increase in San Lorenzo on September 13 in the satellite data. The high NO₂ values remained predominantly confined to the Delta region, traveling with the bulk of the plume on September 13, whereas CO exhibited a broader dispersion, clearly reaching San Lorenzo on this date.

Trajectories of air masses calculated using HYSPLIT (Hybrid Single-Particle Lagrangian Integrated Trajectory) (Draxler and Rolph, 2013; Stein et al., 2015) at various altitudes (20, 500, 1000, 1500, and 2000 m above ground level, m AGL) for both days were analyzed in a previous study (Binet et al., 2024). The analysis showed a direct correlation between the direction of these air masses and the gas plumes observed in the Paraná River Delta fires, which were found to move towards Fighiera on September 13 and over San Lorenzo on September 16, 2022, as previously described for the contamination plumes.

Furthermore, the cited study also investigated the wind directions provided by the weather station at Rosario International Airport 'Islas Malvinas' (32°54'S, 60°47'W - Height: 25 m - Station ID: 87480 - ICAO Code: SAAR), which are in accordance with the emission plumes and air masses' traveling directions for the days of the peaks in gas levels.

3.4.1. Behavior of AOD and aerosol characteristics during the fire period

3.4.2. AOD analysis

The mean AOD values at 470 nm and their respective standard deviations were calculated for the locations of Fighiera and San Lorenzo for the period from September 6 to September 17, 2022 (Fig. 6 a). It is important to note that AOD data from MAIAC/MODIS for September 11, 16, and 17 were unavailable due to cloud cover for both sites. On September 13, 2022, the standard deviation of AOD was notably higher for San Lorenzo compared to Fighiera, suggesting more significant aerosol fluctuations in the former. Interestingly, on September 8, San Lorenzo experienced a marked increase in AOD, which aligns with the rise in optical depth of the Black Carbon fraction seen in Fig. 7. This increase in AOD is attributed to biomass burning events that occurred in Southeastern South America, further analyzed in Valle Seijo et al. (2024). Satellite images from VIIRS S-NPP, captured on September 8, 2022, and September 13, 2022, are included in Appendix A to illustrate the differences in the origins of the plumes generated by these biomass burning events on those dates. For its part, Fighiera experienced an increase in mean AOD on September 12, which is consistent with the patterns shown for Black Carbon in Fig. 7 for the same date and correlates with the fire peak analysis discussed in Table 1.

The spatial distribution of the mean AOD was specifically analyzed for September 13, 2022 (Fig. 6b). On this date, AOD values near 1 were observed in San Lorenzo, aligning well with the arrival of the aerosol plume from burning events, as shown in Fig. 5a (top panel). This figure also details the concentrations of NO_2 and CO detected by TROPOMI/ Sentinel 5-P and shows the zones of higher values of these contaminants while the emissions plume travels in the Northwest direction, as already discussed. High standard deviation values can be observed for

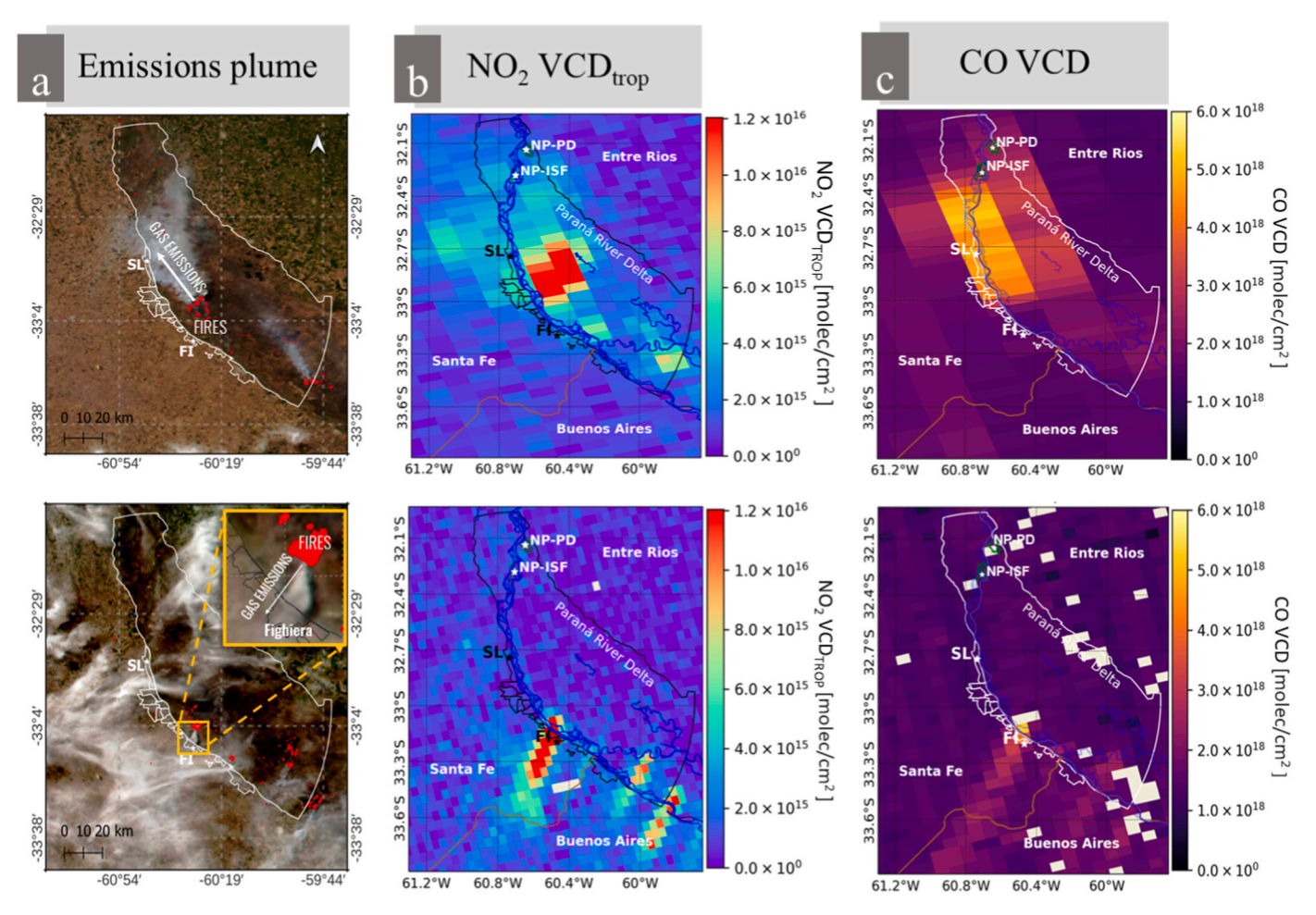


Fig. 5. (a) True color images and heat point locations detected by the VIIRS/SNPP satellite, illustrating the fires in the Paraná Delta. The white arrows indicate the direction of gas emissions from the fires. (b) Tropospheric NO₂ VCD and (c) CO VCD provided by TROPOMI. The top panel shows the situation observed on September 13, 2022, while the bottom panel represents the situation on September 16, 2022.

Table 3
CO VCD and NO₂ VCD_{trop} [both in molecules/cm²] detected by TROPOMI/
Sentinel-5P during the fire events in the Paraná River Delta, in front of the
Greater Rosario coastal region, for the period from September 6 to 17, 2022.

		-	-	-		
	Site	Mean	St. Dev.	MIN	Q3	MAX
NO ₂	Fighiera	3.42×10^{15}	4.69 × 10 ¹⁵	7.95 × 10 ¹⁴	2.86 × 10 ¹⁵	1.66×10^{16}
	San	2.00 ×	1.30 ×	8.79 ×	2.54 ×	4.63 ×
	Lorenzo	10^{15}	10^{15}	10^{14}	10^{15}	10^{15}
CO	Fighiera	1.79×10^{18}	4.34×10^{17}	1.20×10^{18}	$2.15\times\\10^{18}$	2.44×10^{18}
	San Lorenzo	$1.74\times\\10^{18}$	6.42×10^{17}	$1.19\times\\10^{18}$	$1.92\times\atop10^{18}$	$\begin{array}{c} 3.29 \times \\ 10^{18} \end{array}$

September 13 (Fig. 6c), indicating an important variability in aerosol concentrations compatible with the arrival of particles with the plume during the burning episodes in a fluctuating way depending on winds and on the development of the fires.

3.4.3. Black carbon aerosol optical depth (BC AOD)

Fig. 7 illustrates that peak values of Aerosol Optical Depth at 550 nm for the Black Carbon fraction (CAMS reanalysis/Copernicus Earth Observation Program/ECMWF) were recorded on September 8, 2022, at both sites. This increase is also evident, for San Lorenzo in Fig. 6 a, which shows corresponding AOD values. However, this increase is not attributed to the fires in the Paraná Delta but rather to a SALLJ likely transporting aerosols from fires in northern Argentina, as observed using the

JSTAR Mapper application, which utilizes data provided by NOAA. On September 12, a higher concentration was observed in Fighiera compared to San Lorenzo, which can be attributed to biomass burning emissions, as related to the trajectories outlined in Binet et al. (2024). As depicted in Fig. 5 a (top panel), on September 13, 2022, the air mass trajectories from the major fire hotspots were directed towards the Northwest, towards San Lorenzo, coinciding with the observed increase in Black Carbon at this site around September 13–14, 2022.

The spatial and temporal variations in BC AOD detected by CAMS on key dates (e.g., 8, 12, and September 13, 2022) show similar trends to those observed in total AOD (MODIS-MAIAC), NO₂ and CO columns (TROPOMI), as well as in the location and movement of fire emission plumes identified by VIIRS satellite imagery. This general consistency provides qualitative support for the use of CAMS-derived BC AOD in this study as a complementary product. To strengthen this analysis, the establishment of an AERONET station in this region would be highly valuable for validating satellite-derived aerosol products, particularly those related to black carbon and total aerosol optical depth. Such ground-based observations would significantly enhance the reliability of current and future remote sensing analyses in the area.

Table 4 indicates that the mean values of the Black Carbon fraction are comparable between Fighiera and San Lorenzo, with a slight increase in the average AOD for this fraction observed in Fighiera.

3.4.4. Aerosol types and Ångström Exponent evaluation

Using the VIIRS algorithm, Fig. 8a shows the aerosol types detected on September 13, 2022, which are also related to the observations in

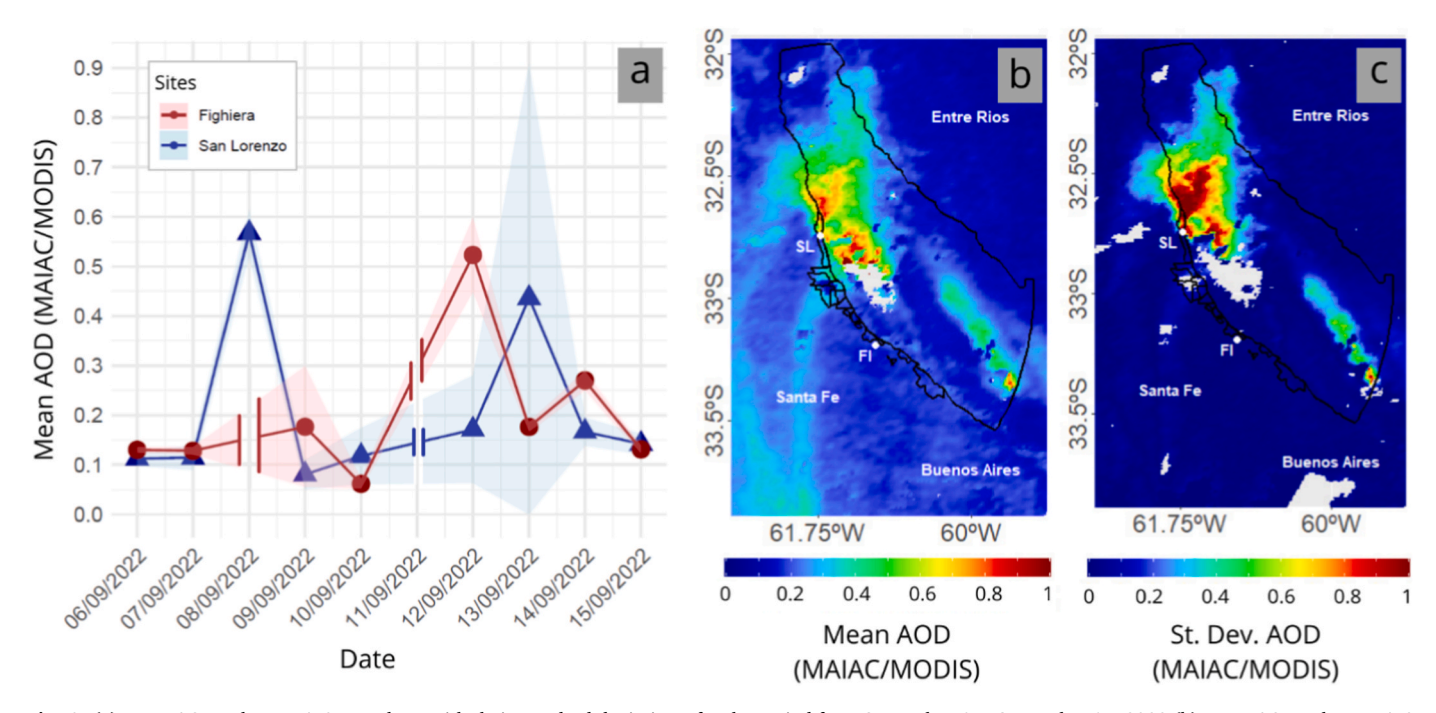


Fig. 6. (a) Mean AOD values at 470 nm, along with their standard deviations, for the period from September 6 to September 17, 2022 (b) Mean AOD values at 470 nm for September 13, 2022. (c) Standard deviation of AOD values at 470 nm for September 13, 2022. Data source: MAIAC-MODIS/NASA.

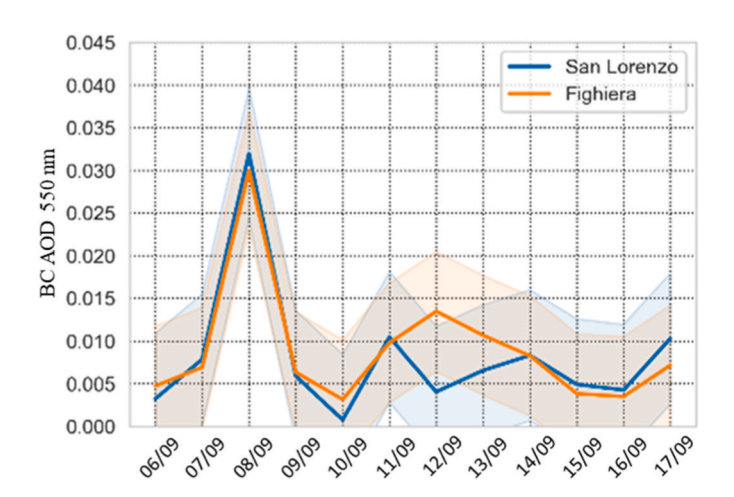


Fig. 7. Forecast values of Aerosol Optical depth at 550 nm for the Black Carbon fraction during the analyzed fire period in the Paraná Delta Islands (CAMS reanalysis/Copernicus Earth observation program/ECMWF). The shaded area represents the standard deviation.

Table 4Descriptive statistics of forecasted AOD at 550 nm for the Black Carbon fraction (CAMS reanalysis/Copernicus Earth observation program/ECMWF) during the analyzed fire period, September 6–17, 2022.

Site	Mean	DV	Q3
Fighiera	0.0089	0.0073	0.0100
San Lorenzo	0.0082	0.0080	0.0088

Fig. 5 (top panel). We included six aerosol categories: mineral dust, smoke, high-altitude smoke, urban/industrial (non-smoke) fine mode, mixed (significant contributions from both fine-mode and coarse-mode aerosols), and background (low-AOD) aerosols. This classification helps primarily identify smoke pixels, which are observed passing over the city of San Lorenzo on that day.

The Ångström Exponent (AE) in Fig. 8b is used to distinguish pixels dominated by coarse-mode particles (such as mineral dust) from other fine-mode particles, including weakly absorbing urban/industrial aerosols (Eck et al., 1999). Comparing the patterns observed in the RGB image in Fig. 5a (top panel), the AOD image of Figs. 6b and 8a, it can be concluded that the high AOD values of Fig. 6b are essentially due to smoke originating in the Delta fires and reaching San Lorenzo. According to Fig. 8b, the retrieved AE values effectively separated fine-mode (high AE) particles over San Lorenzo. Within the fine-mode group, smoke aerosols (indicated in gray) can be further distinguished from non-smoke urban/industrial aerosols (indicated in dark green) detected in Puerto San Martín, an important industrial area.

Fig. 8b clearly distinguish between the areas with predominant normal aerosols of the zone (with smaller Ångström Exponent and thus coarser aerosols) and those with smoke aerosols (finer in size and thus with higher values of the Ångström Exponent, that are compatible with the presence of Black Carbon at Brown Carbon (Hoffer et al., 2006)).

3.5. Comparison of NO₂ VCD_{trop} and CO VCD levels during periods with and without fires: trends in rural versus industrial sites

In Binet et al. (2024), it was observed that the average NO_2 VCD_{trop} values during the fire period studied (September 6–16, 2022) were higher in Fighiera compared to San Lorenzo, with an increase of +71 %. In contrast, for the same period without fires (September 6–16, 2019), San Lorenzo exceeded Fighiera with an increase of +45 %.

Fig. 9-a and 9-b illustrate a general increase in NO_2 VCD_{trop} in FI and SL from September 6 to September 17, 2022, compared to the same period in 2019. In this case, the QA filter >0.75 was not applied due to data scarcity for certain days within the 2019 study period; thus, these graphs provide an approximation. The primary objective is to discern trends in NO_2 VCD across both sites for the specified period. Both in Fighiera (Fig. 9-a) and San Lorenzo (Fig. 9-b), it is evident that NO_2 VCD levels were generally lower during the 2019 period (without Delta Paraná fires) compared to the same period in 2022 (with Delta Paraná fires)

In Fig. 9a, the peak of NO_2 VCD_{trop} occurred on September 16, 2022, when wind direction facilitated the transport of gas emissions from the

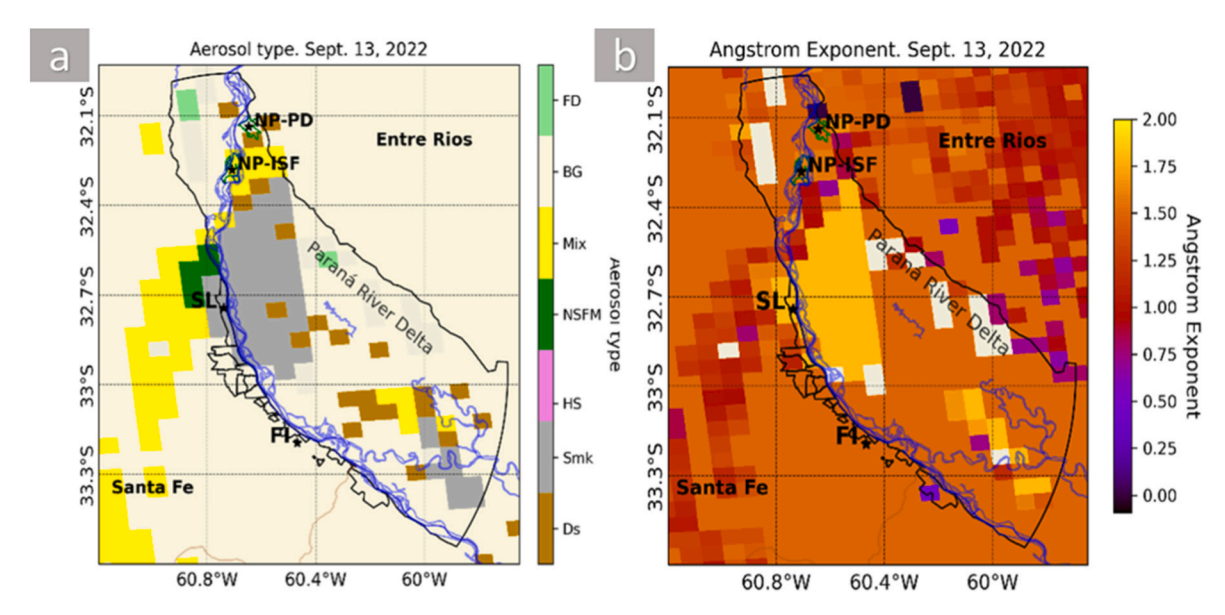


Fig. 8. Smoke event over San Lorenzo on September 13, 2022, as observed in (a) aerosol types retrieved by the VIIRS Deep Blue algorithm. The aerosol classifications include dust (Ds), smoke (Smk), high-altitude smoke (HS), non-smoke fine mode (NSFM), mixed (Mix), background (BG), and fine mode dominated (FD). (b) The corresponding Ångström Exponent retrieved by the VIIRS Deep Blue algorithm. National Parks: Pre-Delta National Park (NP-PD) and Santa Fe Island National Park (NP-ISF).

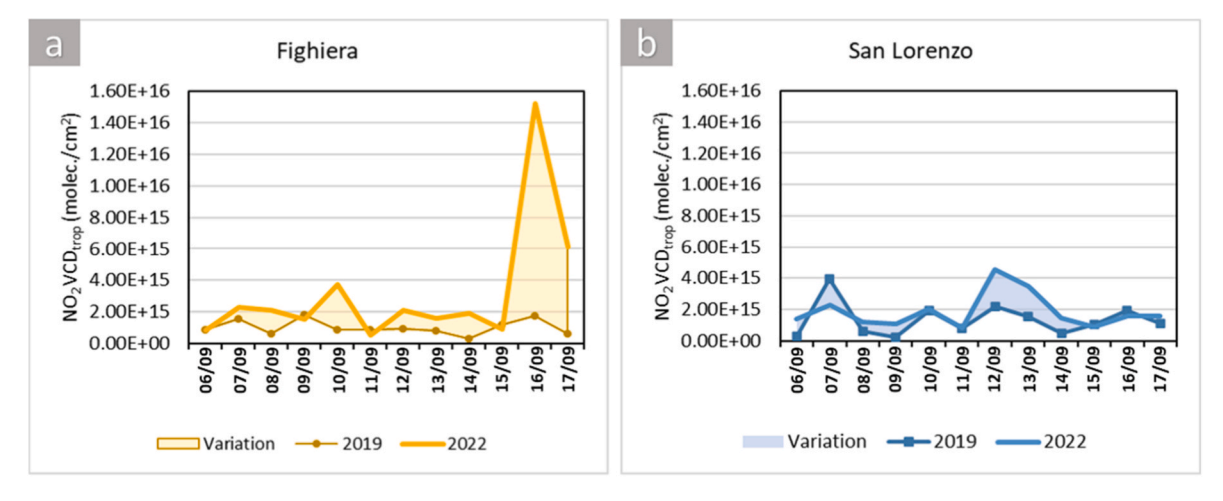


Fig. 9. Variation in daily NO₂ VCD_{trop} detected by TROPOMI in Fighiera and San Lorenzo during the period from September 6 to 17, corresponding to the years 2019 and 2022. (a) Fighiera. (b) San Lorenzo.

delta, directly impacting Fighiera and the surrounding areas.

Particularly, the peak was 8.6 times higher than on the same day in 2019, significantly elevating the average NO_2 VCDtrop values for the entire analyzed period. A similar increase in NO_2 VCD $_{trop}$ is observed in San Lorenzo during this period in 2022, with notable peaks on September 12, 13, and 14 (Fig. 9-b).

The average NO_2 VCDtrop detected in Fighiera from September 6 to 17, 2022, was 3.19 times higher than during the same period in 2019. This substantial increase likely indicates a degradation in air quality associated with the wildfire season. In San Lorenzo, a 37.91 % increase is observed during the same period in 2022 relative to 2019.

To complement the current analysis and provide a more comprehensive view of NO_2 VCD $_{trop}$ in the absence of fires, the analysis was expanded to include entire years. Additionally, CO and AOD were incorporated as variables to enrich the dataset.

Fig. 10 shows that, overall, between 2019 and 2023, $NO_2\ VCD_{trop}$ values are consistently higher in San Lorenzo compared to Fighiera. A cyclical pattern in NO_2 levels is evident, particularly during years with

fewer fire events, such as 2019 and 2023, where a decline in NO_2 is observed during the warmer months, followed by a gradual increase in winter. Fuglestvedt et al. (1999) also observed similar tendencies in the United States, Australia, and certain regions of Europe. This trend may be attributed to the inverse relationship between NO_2 concentrations and solar radiation. As noted by Nguyen et al. (2022), tropospheric ozone forms during the atmospheric NO_x cycle, wherein the photolysis of NO_2 produces atomic oxygen, which reacts with molecular oxygen (O_2) to generate O_3 . The presence of O_3 in the troposphere results from photochemical reactions involving NO_x , VOCs, or CO.

Furthermore, the most significant NO_x emissions arise from fossil fuel combustion processes, which can be classified as stationary or mobile sources (Nguyen et al., 2022). Consequently, the reduced industrial activity and lower traffic volumes in summer may also contribute to the decrease in NO_2 concentrations during this season.

Similar to NO₂, CO is one of the precursors in photochemical ozone formation, so it is reasonable to attribute the lower CO values observed during summer to this process. CO is distinctive in the lower atmosphere

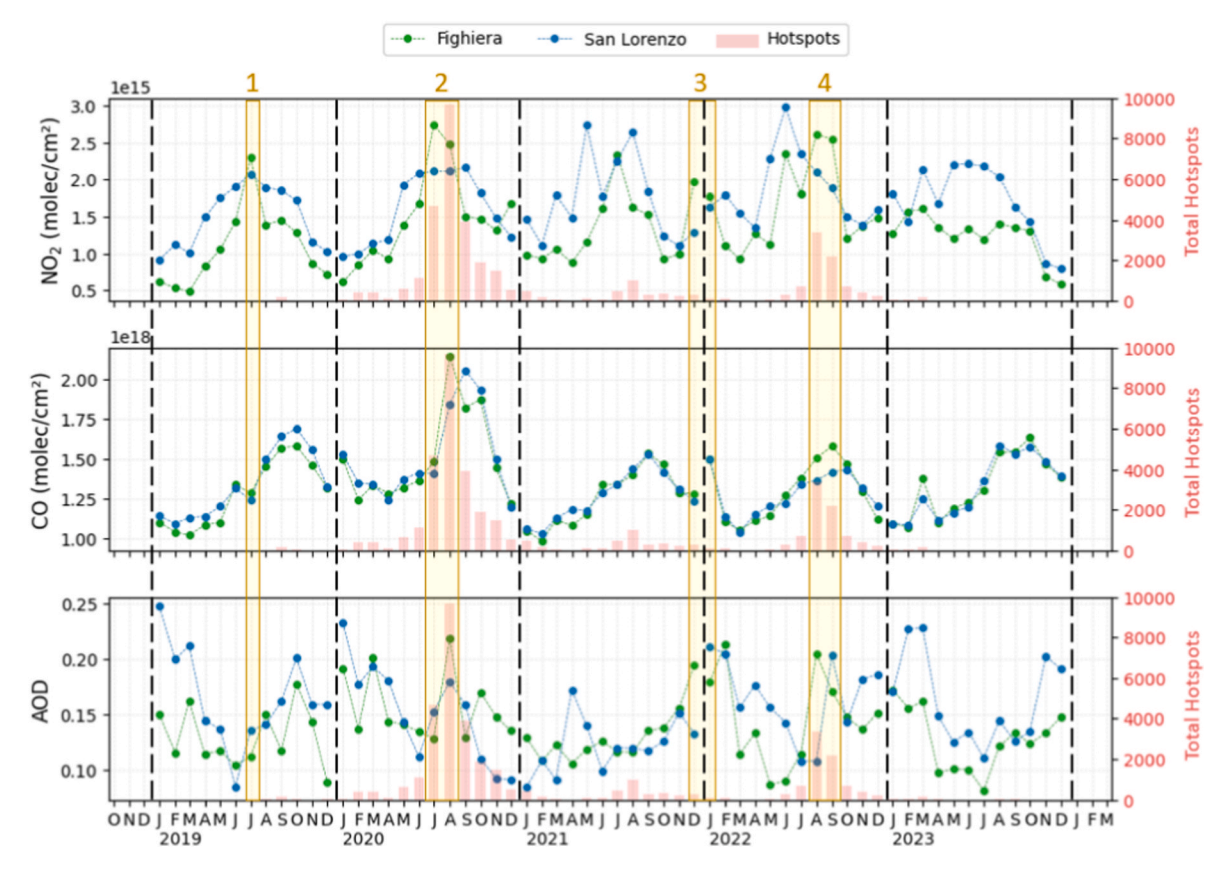


Fig. 10. Time series of monthly NO₂ VCDtrop (TROPOMI), CO VCD (TROPOMI), and AOD (MAIAC) over San Lorenzo and Fighiera. The yellow boxes highlight months where at least one parameter measured in Fighiera exceeded those recorded in San Lorenzo. Black dashed lines indicate the transition between years, while the red bars represent fire hotspots detected by VIIRS/SNPP in the central Paraná Delta region.

because it can persist for around a month, allowing it to travel over long distances (Weigand et al., 2019). This factor makes it possible for this gas to be transported by the SALLJ, which can occur in spring months (Ulke, 2019).

Regarding AOD, although no clear cyclical pattern is observed (as compared to NO₂ and CO), there is a noticeable decrease during the autumn-winter months, followed by a progressive increase throughout the spring-summer period. These findings align with those reported by Della Ceca et al. (2018), where the highest absolute AOD values were recorded between August and October in an Argentinian region comparable to the one of the present analysis and located approximately 300 km away from our study site. The study further highlights that these increases in AOD values are primarily driven by biomass burning (BB) emissions at both local and continental scales (e.g., Argañaraz et al., 2015; Ulke et al., 2011). Videla et al., 2013 estimated that during the burning season, fires in nearby regions—mainly in the Chaco woodlands of Argentina and Paraguay—contribute 60-70 % of the BB-related AOD in central Argentina, while the remaining 30-40 % is largely attributed to long-range transport of emissions from the Brazilian Amazon and Cerrado regions.

Despite the traditional, cyclical, and characteristic behavior of each variable analyzed, it is worth noting that all three variables behave similarly during fire seasons. In other words, each variable breaks its typical cycle to reflect the impact of the fires. This effect is particularly evident in yellow boxes 2 and 4 of Fig. 10, which represent July and August 2020, and August and September 2022, respectively. Periods of extreme drought when fire hotspots in the Paraná Delta Islands reached up to 9720 hotspots detected by the VIIRS/SNPP sensor (in August 2020). These cases demonstrate how, under fire conditions in the Paraná Delta, NO₂, CO, and AOD values in a rural area (Fighiera) can exceed those in an industrial area (San Lorenzo). On the other hand, in the case

of Yellow Box 1, which predominantly corresponds to July 2019, the observed increases in NO $_2$ VCD $_{trop}$ values are not attributed to the Paraná River fires. Instead, they are linked to air mass flows from the northeast, which transported NO $_2$ emissions originating from the City of Buenos Aires (with a population of 3.12 million according to INDEC, 2022). This influx of pollutants raised the standard deviation for this period, with Fighiera recording a value of 2.8 \times 10 15 molecules/cm 2 , the highest standard deviation observed in 2019. An increase in AOD values is observed in Box N°3, despite the low number of detected hotspots within the study area. This rise in AOD is likely linked to fires that occurred during the same period in Corrientes Province, located 313 km Northeast of our study site. According to Saucedo et al. (2023), these fires impacted approximately 12 % of the province's total area, with wetlands being the most severely affected.

In Fig. 11, the correlation among the different variables under study (FRP, total number of hotspots, AOD at 470 nm, NO_2 VCD $_{trop}$, and CO VCD) is presented for the months with the highest wildfire intensity in the Paraná River Delta, as previously shown in Fig. 10.

Both panels (Fig. 11a and b) show that all analyzed variables exhibit positive correlations. The strongest associations were observed between AOD and CO VCD, with correlation coefficients of r=0.75~(p=0.000) in Fighiera and r=0.64~(p=0.000) in San Lorenzo. When comparing both sites, Fighiera generally displayed stronger correlations between gaseous pollutants and aerosols. Although the correlation values were moderate, significant associations were identified between AOD and $NO_2~VCD_{trop}~(r=0.55)$, as well as between CO VCD and $NO_2~VCD_{trop}~(r=0.40)$.

The correlation between FRP and trace gases was relatively weak at both sites, likely influenced by wind direction during fire events and the spatial distance between the measurement locations and the fire sources. However, slightly higher correlations between FRP and the remaining

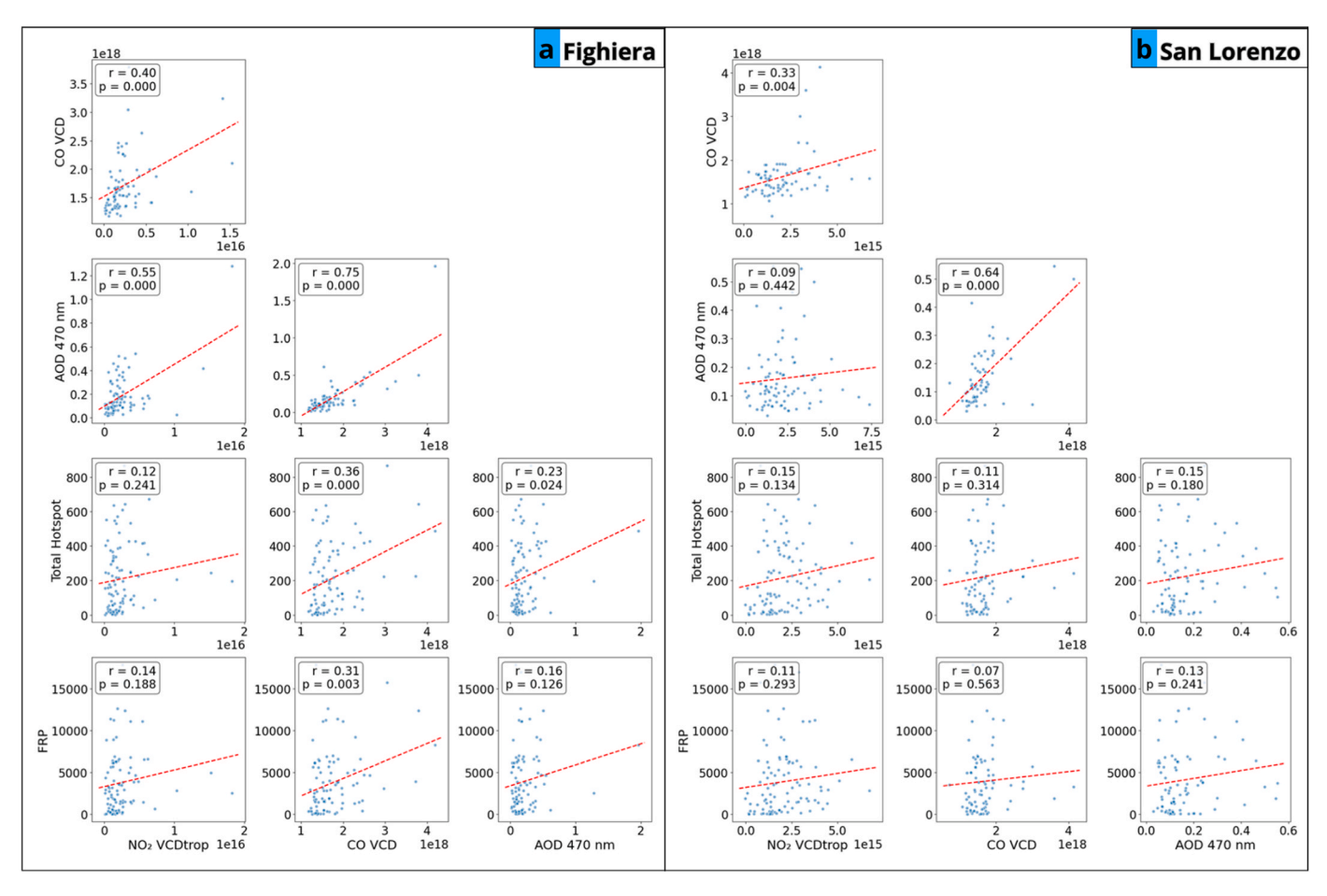


Fig. 11. Correlation between Fire Radiative Power (FRP), total number of hotspots, Aerosol Optical Depth at 470 nm (AOD 470 nm), tropospheric NO₂ column density (NO₂ VCD_{trop}), and CO column density (CO VCD). The analysis focuses on the periods of highest wildfire activity in the Paraná River Delta, specifically July–September of 2020, and August–September of 2022. The variables were retrieved from VIIRS/S-NPP (FRP and hotspot count), TROPOMI/Sentinel-5P (NO₂ VCD_{trop} and CO VCD), and MAIAC/MODIS (AOD at 470 nm). Each subplot shows the Pearson correlation coefficient (r) and its associated p-value (p), alongside a linear regression line (dashed red) fitted to the data. Green arrows indicate the strongest and most statistically significant correlations at each site (p < 0.05 and r > 0.40).

variables were observed in Fighiera compared to San Lorenzo, which may be explained by Fighiera's closer proximity to the main fire fronts. Indeed, the most intense wildfire activity in the Paraná River Delta tends to concentrate in areas adjacent to Fighiera.

4. Conclusion

This study highlights the substantial effects that biomass burning in the Paraná River Delta has on air quality in adjacent rural and industrial areas, specifically in the coastal areas of the towns of Fighiera and San Lorenzo. Differences in $\mathrm{NO_2}$ VCD $_{\mathrm{trop}}$ and CO VCD levels were observed between the northern (San Lorenzo) and southern (Fighiera) areas of Gran Rosario, with critical days for each location that aligned with wind directions from the extensive fire zones. Notably, $\mathrm{NO_2}$ VCD $_{\mathrm{trop}}$ and CO VCD levels detected in Fighiera exceeded those in San Lorenzo on certain days, an unusual finding considering the industrial activities of the latter.

The maps of mean AOD values obtained from MAIAC-NASA showed a strong correlation with NO_2 and CO maps from TROPOMI/Sentinel-5P satellite data, particularly on September 13, 2022. Peak AOD values were recorded on September 8 in San Lorenzo and on September 12 in Fighiera, consistent with the optical depth results for Black Carbon aerosols.

Significant impacts on air quality were observed in both urban and rural areas, with atmospheric pollutant levels far exceeding those during non-fire periods. On certain days, the rural population of Fighiera, located close to large fire hotspots, experienced higher pollutant levels than the industrial town of San Lorenzo, underscoring the overwhelming impact of fires, which can overshadow other local emission sources.

The topography of the study area presents minimal altitudinal variation and lacks major orographic barriers that could significantly influence surface atmospheric circulation. However, it is worth noting that the region is situated within the influence of the SALLJ, which may contribute to the long-range transport of atmospheric pollutants from distant sources.

Therefore, it is important to acknowledge that air quality at the study sites may be influenced not only by fires in the Paraná Delta, but also by those in other regions of Argentina, including the Gran Chaco and Corrientes. Moreover, large-scale atmospheric transport mechanisms, such as the SALLJ, can carry gaseous pollutants and particulate matter from more distant areas, notably the Amazon rainforest and Paraguay.

Although this study focuses on a specific period and region, the methodology (combining multi-sensor satellite data with backward trajectory analysis) can be applied to investigate fire-related pollution events in other regions with similar topographic characteristics, particularly flat areas. For example, it could be used to assess the impact of wildfires in the Gran Chaco region, whose emissions may affect cities such as Resistencia.

These findings underscore the urgent need for effective fire management and rapid mitigation strategies to reduce the adverse impacts

on public health and the environment. Even if air quality detection systems in the country or province have not yet expanded to cover sensitive areas—such as those frequently affected by pollutant gases and aerosols generated by intense fires—we expect, in the near future, to receive both national and international support from research groups and institutions (as has occurred in the past in other contexts) to install sensors for atmospheric gases and particles. This will enable the integration of ground-based measurements with satellite-derived observations.

CRediT authorship contribution statement

M.V. Binet: Writing – review & editing, Writing – original draft, Visualization, Software, Methodology, Investigation, Formal analysis, Data curation, Conceptualization. G.A. Piñol: Writing – review & editing, Writing – original draft, Software, Methodology, Investigation, Formal analysis, Data curation, Conceptualization. M.F. Valle Seijo: Writing – review & editing, Writing – original draft, Visualization, Software, Methodology, Investigation, Formal analysis, Data curation, Conceptualization. M.I. Micheletti: Writing – review & editing, Validation, Supervision, Resources, Project administration. R.D. Piacentini: Writing – review & editing, Visualization, Supervision, Resources.

Declaration of competing interest

The authors declare that they have no known competing financial interests or personal relationships that could have appeared to influence the work reported in this paper.

Acknowledgements

We acknowledge the following Argentine institutions: CONICET and the National University of Rosario. We also extend our gratitude to the TROPOMI S5P, VIIRS, and MODIS teams from ESA, NOAA, and NASA for their high-quality work and the maintenance of the databases utilized in this study. Additionally, we acknowledge ECMWF for providing ERA5 and CAMS data available through the Copernicus Climate Data Store (https://cds.climate.copernicus.eu/).

Appendix A. Supplementary data

Supplementary data to this article can be found online at https://doi.org/10.1016/j.apr.2025.102712.

References

- Argañaraz, J.P., Gavier Pizarro, G., Zak, M., et al., 2015. Fire Regime, Climate, and Vegetation in the Sierras de Córdoba, Argentina. fire ecol 11, 55–73. https://doi.org/ 10.4996/fireecology.1101055.
- Binet, M.V., Micheletti, M.I., Piacentini, R.D., 2024. Propagation of NO₂ originated in intense fires in the Paraná River Delta analyzed from satellite observations. Adv. Space Res. 74 (2), 682–694. https://doi.org/10.1016/j.asr.2024.04.030.
- Borsdorff, T., et al., 2018. Mapping carbon monoxide pollution from space down to city scales with daily global coverage. Atmos. Meas. Tech. 11 (10), 5507–5518. https:// doi.org/10.5194/amt-11-5507-2018.
- Brook, R.D., et al., 2010. Particulate matter air pollution and cardiovascular disease: an update to the scientific statement from the American Heart Association. Circulation 121 (21), 2331–2378. https://doi.org/10.1161/CIR.0b013e3181dbece1.
- Casanova, R., et al., 2016. A voxel-based morphometry study reveals local brain structural alterations associated with ambient fine particles in older women. Front. Hum. Neurosci. 10. https://doi.org/10.3389/fnhum.2016.00319.
- Della Ceca, L.S., Ferreyra, M.F.G., Lyapustin, A., Chudnovsky, A., Otero, L.A., Carreras, H.A., et al., 2018. Satellite-based view of the aerosol spatial and temporal variability in the córdoba region (Argentina) using over ten years of high-resolution data. ISPRS J. Photogrammetry Remote Sens. 145, 250–267. https://doi.org/ 10.1016/j.isprsiprs.2018.08.016.
- Draxler, R.R., Rolph, G.D., 2013. HYSPLIT (HYbrid Single-Particle Lagrangian Integrated Trajectory). Model Access via NOAA ARL READY Website. NOAA Air Resources Laboratory, College Park, MD. Recuperado de. https://www.ready.noaa.gov/HY SPLIT.php.

- Eck, T.F., Holben, B.N., Reid, J.S., Dubovik, O., Smirnov, A., O'Neill, N.T., et al., 1999. Wavelength dependence of the optical depth of biomass burning, urban, and desert dust aerosols. J. Geophys. Res. 104 (D24). https://doi.org/10.1029/1999JD900923, 31.333-31.349.
- Fuglestvedt, J.S., Berntsen, T.K., Isaksen, I.S.A., et al., 1999. Climatic forcing of nitrogen oxides through changes in tropospheric ozone and methane; global 3d model studies. Atmos. Environ. 33, 961–977. https://doi.org/10.1016/S1352-2310(98)00217-9.
- Ghasempour, F., Sekertekin, A., Kutoglu, S.H., 2021. Google Earth Engine based spatio-temporal analysis of air pollutants before and during the first wave COVID-19 outbreak over Turkey via remote sensing. J. Clean. Prod. https://doi.org/10.1016/j.iclepro.2021.128599.
- Guerrero, F., Espinoza, L., Vidal, V., Carmona, C., Krecl, P., et al., 2024. Black carbon and particulate matter concentrations amid central Chile's extreme wildfires. Sci. Total Environ. 951, 175541. https://doi.org/10.1016/j.scitotenv.2024.175541.
- Hersbach, H., Bell, B., Berrisford, P., Biavati, G., Horányi, A., Muñoz Sabater, J., Nicolas, J., Peubey, C., Radu, R., Rozum, I., Schepers, D., Simmons, A., Soci, C., Dee, D., Thépaut, J.-N., 2023. ERA5 hourly data on pressure levels from 1940 to present. Copernicus Climate Change Service (C3S) Climate Data Store (CDS). https://doi.org/10.24381/cds.bd0915c6.
- Hoffer, A., Gelencser, A., Guyon, P., Kiss, G., Schmid, O., Frank, G., Artaxo, P., Andreae, M.O., 2006. Optical properties of humic-like substances (HULIS) in biomass-burning aerosols. Atmos. Chem. Phys. 6, 3563–3570.
- Inness, A., et al., 2019. The CAMS reanalysis of atmospheric composition. Atmos. Chem. Phys. 19, 3515–3556. https://doi.org/10.5194/acp-19-3515-2019.
- Junk, W.J., An, S., Finlayson, C.M., Gopal, B., Květ, J., Mitchell, S.A., Mitsch, W.J., Robarts, R.D., 2013. Current state of knowledge regarding the world's wetlands and their future under global climate change: a synthesis. Aquat. Sci. 75, 151–167. https://doi.org/10.1007/s00027-012-0278-z.
- Kaiser, J.W., et al., 2012. Biomass burning emissions estimated with a global fire assimilation system based on observed fire radiative power. Biogeosciences 9 (2), 527–554. https://doi.org/10.5194/bg-9-527-2012.
- Landgraf, J., et al., 2016a. Carbon monoxide total column retrievals from TROPOMI shortwave infrared measurements. Atmos. Meas. Tech. 9 (10), 4955–4975. https://doi.org/10.5194/amt-9-4955-2016.
- Landgraf, J., aan de Brugh, J., Scheepmaker, R., Borsdorff, T., Hu, H., Houweling, S., Butz, A., Aben, I., Hasekamp, 2016b. O.: carbon monoxide total column retrievals from TROPOMI shortwave infrared measurements. Atmos. Meas. Tech. 9, 4955–4975. https://doi.org/10.5194/amt-9-4955-2016.
- Lyapustin, A., et al., 2011. Multiangle implementation of atmospheric correction (MAIAC): 2. Aerosol algorithm. J. Geophys. Res. 116 (D3), D03211. https://doi.org/ 10.1029/2010JD014986.
- Lyapustin, A., Wang, Y., Laszlo, I., Korkin, S., 2012. Improved cloud and snow screening in MAIAC aerosol retrievals using spectral and spatial analysis. Atmos. Meas. Tech. 5 (4), 843–850. https://doi.org/10.5194/amt-5-843-2012.
- Lyapustin, A., Wang, Y., Korkin, S., Huang, D., 2018. MODIS Collection 6 MAIAC algorithm. Atmos. Meas. Tech. 11 (10), 5741–5765. https://doi.org/10.5194/amt-11-5741-2018.
- Muñoz Sabater, J., 2019. ERA5-Land hourly data from 1950 to present. Copernicus Climate Change Service (C3S) Climate Data Store (CDS). https://doi.org/10.24381/ cds.e2161bac.
- National Meteorological Service, 2020. El Niño-southern oscillation (ENSO) October 2020. Technical Report National Weather Service Argentina.
- National Meteorological Service, 2022. The winter of 2022 was the 7th driest in 61 years. National Meteorological Service. https://www.smn.gob.ar/noticias/el-invierno-20 22-fue-el-7%C2%B0-m%C3%A1s-seco-en-61-a%C3%B1os.
- Nguyen, D.-H., Lin, C., Vu, C.-T., Cheruiyot, N.K., Nguyen, M.K., Le, T.H., Lukkhasorn, W., Vo, T.-D.-H., Bui, X.-T., 2022. Tropospheric ozone and NOx: a review of worldwide variation and meteorological influences. Environ. Technol. Innovat. 28, 102809. https://doi.org/10.1016/j.eti.2022.102809.
- Oelker, J., Losa, S., Richter, A., et al., 2022. TROPOMI-retrieved underwater light attenuation in three spectral regions in the ultraviolet and blue. Front. Mar. Sci. 9, 787–992. https://doi.org/10.3389/fmars.2022.787992.
- Saucedo, G.I., Perucca, R., Kurtz, D., 2023. Las causas de los incendios de principios del año 2022 en la provincia de Corrientes. Ecol. Austral 33 (1), 273–284. https://d oi/10.25260/EA.23.33.1.0.2020.
- Stein, A.F., Draxler, R.R., Rolph, G.D., et al., 2015. Noaa's hysplit atmospheric transport and dispersion modeling system. Bull. Am. Meteorol. Soc. 17, 2059–2077. https:// doi.org/10.1175/BAMS-D-14-00110.1.
- Tang, W., Llort, J., Weis, J., et al., 2021. Widespread phytoplankton blooms triggered by 2019–2020 Australian wildfires. Nature 597, 370–375. https://doi.org/10.1038/ s41586-021-03805-8.
- Ulke, Ana G., 2019. Influence of regional transport mechanisms on the fingerprint of biomass-burning aerosols in Buenos Aires. Adv. Meteorol. 2019 (6792161), 13. https://doi.org/10.1155/2019/6792161.
- Ulke, Ana G., Maria, K., de Freitas, S.R., 2011. Biomass Burning in South America: Transport Patterns and Impacts. InTech. https://doi.org/10.5772/19264.
- Urbanski, S., 2014. Wildland fire emissions, carbon, and climate: emission factors. For. Ecol. Manag. 317, 51–60. https://doi.org/10.1016/j.foreco.2013.05.045.
- Valle Seijo, M.F., Otero, L.A., Piacentini, R.D., 2024. Spatio-temporal analysis of fire events over the past 10 Years in the central-East region of Argentina and surrounding areas. 2024. IEEE Biennial Congress of Argentina (ARGENCON) 1–8. https://doi. org/10.1109/ARGENCON62399.2024.10735824.
- Veefkind, J., Aben, I., McMullan, K., et al., 2012. TROPOMI on the esa sentinel-5 precursor: a gmes mission for global observations of the atmospheric composition for climate, air quality and ozone layer application. Remote Sens. Environ. 120, 70–83. https://doi.org/10.1016/j.rse.2011.09.027.

ARTICLE IN PRESS

M.V. Binet et al.

Atmospheric Pollution Research xxx (xxxx) xxx

- Videla, F.H.C., Barnaba, F., Angelini, F., Cremades, P., Gobbi, G.P., 2013. The relative role of amazonian and non-amazonian fires in building up the aerosol optical depth in south America: a five year study (2005–2009). Atmos. Res. 122, 298–309. https:// doi.org/10.1016/j.atmosres.2012.10.026.
- Wan, N., et al., 2023. Estimation of biomass burning emission of NO₂ and CO from 2019–2020 Australia fires based on satellite observations. Atmos. Chem. Phys. 23 (1), 711–724. https://doi.org/10.5194/acp-23-711-2023.
- Weigand, M., Wurm, M., Dech, S., Taubenböck, H., 2019. Remote sensing in environmental justice research—a review. ISPRS Int. J. GeoInf. 8, 20. https://doi. org/10.3390/ijgi8010020.
- Wooster, M.J., et al., 2003. Fire radiative energy for quantitative study of biomass burning: derivation from the BIRD experimental satellite and comparison to MODIS fire products. Rem. Sens. Environ. 86 (1), 83–107. https://doi.org/10.1016/S0034-4257(03)00070.1